INTERNATIONAL JOURNAL FOR NUMERICAL AND ANALYTICAL METHODS IN GEOMECHANICS
Int. J. Numer. Anal. Meth. Geomech., **23**, 1495–1519 (1999)

STRESS–STRAIN ANALYSIS IN PRODUCTIVE GAS/OIL RESERVOIRS

GIUSEPPE GAMBOLATI, PIETRO TEATINI AND LUCIO TOMASI

Department of Mathematical Methods and Models for Scientific Applications (DMMMSA), Università degli Studi di Padova, Via Belzoni 7, 35131 Padova, Italy

SUMMARY

A numerical study of the stress–strain distribution in a thin disc-shaped reservoir embedded in a poro-elastic half-space and subject to a unit pore pressure decline is presented. The results are then compared with those of a geometrically equivalent porous cylindrical body which is either free to or prevented from expanding laterally (oedometric analogy). The analysis is based on the linear theory of poro-elasticity solved with the aid of the finite element method. The strength source is provided by the pressure gradient generated in a small region surrounding the gas/oil field where pore pressure dissipates. The influence of the burial depth c is also investigated. The results show that the reservoir rock undergoes a vertical compaction δ which is independent of c and very close to the compaction of the equivalent confined cylinder. The confinement factor is also similar. The horizontal displacement is, however, much larger. Its maximum value occurs at the boundary of the field and is of the same order of magnitude as δ. In addition, at the outer reservoir margin shear stresses develop which are totally missing in both the free and the constrained cylinders. It is shown that the vertical displacements of reservoir top and bottom, as well as the radial ones, are sensitive to c, especially in shallow formations. Finally, the largest shear stress is found to be related to the magnitude of the pressure gradient, i.e. to the radial size of the neighbouring volume where pore pressure vanishes.

KEY WORDS: land subsidence; gas/oil reservoirs; poro-elasticity; stress–strain distribution

1. INTRODUCTION

It is well recognized that rock mechanical properties play a key role in controlling the actual volume of the land subsidence bowl which is caused by fluid withdrawal from gas/oil fields. While during the reservoir production life representative compaction data may be obtained from the installation of radioactive bullets (the so-called markers) within the mineralized formations, at the planning and inception stages the evaluation of the rock parameters is generally based on laboratory tests performed on material samples, taken from exploratory boreholes. To obtain realistic settlement predictions the essential requirement is that the stress–strain path followed by the samples in the laboratory experiments be the same as the one experienced by the stressed sediments in the reservoir. Generally, uni-axial vertical strain of the fluid bearing formations is assumed and, as a major consequence, the vertical soil compressibility derived from oedometer

* Correspondence to: G. Gambolati, DMMMSA, Università degli Studi di Padova, Via Belzoni 7, 35131 Padova, Italy

Contract grant sponsor: EC Environment Research Programme; contract grant number: EV5V-CT94-0498, Climatology and Natural Hazards

CCC 0363–9061/99/131495–25$17.50 *Received 24 October 1997*
Revised 31 August 1998

trials is considered to be the fundamental mechanical property characterizing the *in situ* rock behaviour. '*A large ratio of lateral extent to vertical thickness … means that compaction will occur largely in the vertical direction with minimal horizontal displacements. Tests to simulate compaction in the subsurface should be confined tests that prevent the rock from undergoing any lateral deformation*' [Reference 1, p. 717]. Similarly, other authors observe that '*sample response during uniaxial-strain testing more closely represents the response of the reservoir rock during compaction and is the primary input in the numerical simulations*' [Reference 2, p. 741].

One of the objectives of the present analysis is to theoretically investigate the validity of this assumption in thin disc-shaped reservoirs embedded in a semi-infinite porous medium at different burial depth and to compare the stresses and deformations which develop because of pore pressure decline with those generated in an ideal oedometric experiment performed over a cylindrical sample with the same geometrical size as the reservoir. For the sake of completeness, the analysis is also extended to a cylindrical porous body which undergoes a similar pore pressure reduction but is free to contract laterally.

Use will be made of a classical poro-elastic theory with a strength source specified *a priori*[3,5] and solved with the aid of the finite element method.[6–9] It has been shown[7] that an accurate determination of the mechanical rock properties above the reservoir, the waterdrive and the confining shales is not really required for the purpose of realistically predicting the land settlement due to gas/oil removal since the primary role is played by the sediments where depressurization takes place. Hence, the importance of laboratory tests able to reproduce the actual *in situ* deformations of the stressed sediments.

The present study will not only focus on the similarities between the reservoir and the equivalent oedometer cell but also on the differences of some stress and strain components (e.g. shear stress and horizontal displacement). The analysis will be extended to include the influence of both burial depth and radial size of the lateral medium where the reference pore pressure is assumed to dissipate, on the stress–strain conditions within the reservoir.

The paper is organized as follows. The basic theory for a poro-elastic body is first briefly reviewed with the solution approach outlined. The assumptions underlying the numerical study are discussed, and in particular the size of a representative reservoir is defined. Then the most salient results are presented. These concern the variables of interest within the gas/oil field and the equivalent poro-elastic rock bodies, i.e. the vertical, radial, tangential and shear stresses, the vertical reservoir top and bottom displacements, the related compaction, the horizontal movement, and the effect of burial depth and pressure gradient magnitude. A set of conclusive remarks are finally issued.

2. OUTLINE OF BASIC THEORY AND SELECTION OF PARAMETERS FOR THE NUMERICAL STUDY

The linear poro-elastic theory is frequently used to predict land settlement over productive gas/oil fields (see, for example, References [8, 9, 10–16]). For the analysis developed in the present paper the possible non-linear rock behaviour has a little relevance vis a vis the nature of the expected results. The basic assumptions underlying the formulation that follows are:

(1) the rock skeleton behaves elastically in the range of linear elasticity;
(2) rock matrix displacements and deformations are small;
(3) individual grains are incompressible;
(4) Terzaghi effective integranular stress principle holds.

The equilibrium equations for a mechanically isotropic porous medium may be written as[17–19]

$$G\nabla^2 u_x + (\lambda + G)\frac{\partial \varepsilon}{\partial x} = \frac{\partial p}{\partial x}$$

$$G\nabla^2 u_y + (\lambda + G)\frac{\partial \varepsilon}{\partial y} = \frac{\partial p}{\partial y} \tag{1}$$

$$G\nabla^2 u_z + (\lambda + G)\frac{\partial \varepsilon}{\partial z} = \frac{\partial p}{\partial z}$$

where $G = E/2(1 + v)$ is the bulk shear or rigidity modulus, E the bulk Young modulus, v the bulk Poisson ratio, $\lambda = vE/(1 - 2v)(1 + v)$ the Lamè constant, $\nabla^2 = \partial^2/\partial x^2 + \partial^2/\partial y^2 + \partial^2/\partial z^2$ the Laplace operator, ε the volume strain or dilatation, p the incremental pore pressure or pore pressure variation, assumed to be prescribed, and x, y, z are the principal co-ordinate directions with z positive downward.

Equations (1) are supplemented by appropriate boundary conditions. In the presence of radial symmetry with r the radial distance, they read (Figure 1):

1. *Free cylinder*:
   $u_r(0, z) = 0$
   $u_z(r, \bar{z}) = 0 \quad \bar{z} = h + 2s_V$
   $\sigma_z(r, 0) = \tau_{zr}(r, 0) = 0$
   $\sigma_r(R_e + s_L, z) = \tau_{rz}(R_e + s_L, z) = 0$
2. *Constrained cylinder*:
   $u_r(0, z) = 0$
   $u_r(R_e + s_L, z) = 0$
   $u_z(r, \bar{z}) = 0$
   $\sigma_z(r, 0) = \tau_{zr}(r, 0) = 0$
3. *Reservoir embedded in a half-space*:
   $\sigma_z(r, 0) = \tau_{zr}(r, 0) = 0$
   $u_r(0, z) = 0$
   $u_r = u_z = 0 \quad \text{at } r, z \to \infty$

We assume $p = -10^4\ \text{kg/m}^2$ within the reservoir and the equivalent cylindrical bodies. The pore pressure dissipates linearly along the segments s_V and s_L in the vertical and horizontal direction, respectively (Figure 1), and is zero in the remainder of the semi-infinite medium. Unless otherwise specified, we simulate a reservoir with $s_L = s_V \ll h$, i.e. the pressure change is assumed to occur in a much smaller volume than the gas/oil field itself. For numerical reasons this volume can never be taken equal to zero, namely in the finite element solution of our poro-elastic problems both s_L and s_V take on some small but finite value. This is needed in order to generate a numerically bounded pressure gradient. The study is performed for the following parameter set (see Figure 1):

$h = 50$ m reservoir thickness
$R_e = 2000$ m outer reservoir radius
$s_L = s_V = 1$ m length over which pore pressure dissipates

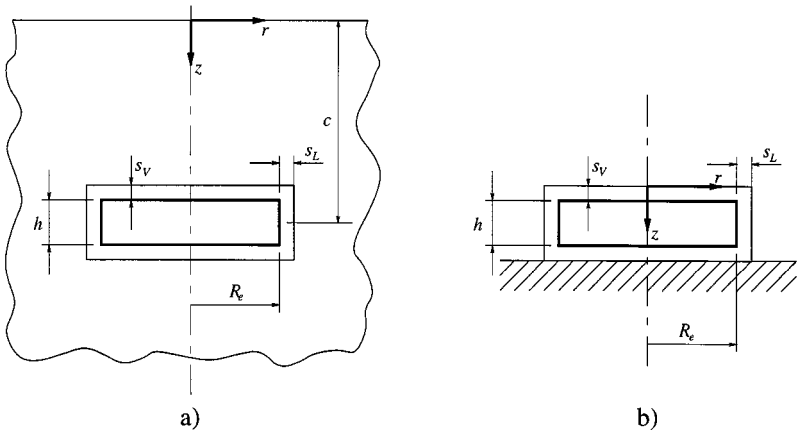

Figure 1. Reservoir embedded in a half-space (a) and equivalent porous cylinder resting on a rigid basement (b)

$\alpha = \dfrac{1}{E}\dfrac{(1+v)(1-2v)}{1-v} = 10^{-6}\ \mathrm{m^2/kg}$ vertical bulk compressibility

$v = 0{\cdot}25$ Poisson ratio of porous medium

The numerical representation of the half-space is obtained with a finite system whose radial and vertical dimension is $\hat{r} = 28\,000$ m and $\hat{z} = 20\,500$ m, respectively. On the boundary of this body we apply the boundary conditions which theoretically apply at infinity. The burial depth c is assumed to vary from $c = 26$ to 3000 m with the intermediate values $c = 100$ and 1500 m. For the latter case ($c = 1500$ m) we investigate the structural response for $s_L = 10$ m and $s_L = 50$ m as well.

Due to radial symmetry the porous systems are subdivided into annular elements of triangular cross-section and equations (1) are integrated by the finite element method where the radial distance r in the integral extended over each single triangle is replaced by a constant value $\bar{r}$, $\bar{r}$ being the radial co-ordinate of the triangle gravity centre.[6] This approximation introduces some errors in the vicinity of the symmetry axis, i.e. in the centre of the reservoir.

The mesh is much refined close to the reservoir boundary where the pore pressure gradient is very large. In any case the mesh refinement has been progressively increased to make sure that both strains and stresses, especially in the area where the strength source is located, converge to stable values and are not affected by significant numerical errors. This has required in some simulations a number of nodes as large as 30 000. It goes without saying that stresses are influenced by the magnitude of the pressure gradient (which depends on s_L) only locally in the vicinity of the field boundary. At some distance from the boundary the stress distribution is insensitive to pressure gradient.

3. RESULTS

In the sequel, we will show and discuss the most significant results obtained from the present study in terms of both medium stresses and deformations and will emphasize the similarities as

well as the differences between the reservoir behaviour on one side and the behaviour of the free and confined cylinders on the other. We assume a positive tensile stress. The shear stress is positive when it is directed in accordance with the positive co-ordinate direction on a plane with positive outer normal, i.e. with an outer normal which has the same verse as the corresponding r or z-axis. It should be observed that in the figures that follow the (small) peak values characterizing the behaviour of stresses and strains at $r = 0$ are the result of the approximation in the local stiffness matrices implied by the use of $\bar{r}$ (see the previous section). Actually, the behaviour of any of the quantities shown is completely flat for $r \to 0$. Depth of burial c is set at a value of 1500 m.

3.1. *Vertical stress* σ_z

Figure 2 shows the behaviour of σ_z vs. r on the median plane for the three sample problems. Figures 3 and 4 provide σ_z vs. z for various distances r from the symmetry axis. Inspection of Figures 2–4 reveals the following:

(1) the vertical stress σ_z within the reservoir/cylinder is the same irrespective of problem and is equal to -10^4 kg/m^2, i.e. the pore pressure decline p. This holds for the reservoir as well except in a limited region close to $r = R_e$ where σ_z turns out to vary between 0·8 and 0·9p. The radial size of this region is a few times the reservoir thickness h (Figure 2). At $r = R_e$ $\sigma_z \sim 0{\cdot}5p$ (Figure 4);
(2) the behaviour of σ_z within the reservoir/cylinder is practically uniform with z;
(3) the vertical stress variation induced in the remaining medium by pore pressure decline within the reservoir is negligible (Figure 4).

3.2. *Radial stress* σ_r *and tangential stress* σ_ϑ

Radial and tangential stresses σ_r and σ_ϑ vs. r on the median plane of the depressurized volume are shown in Figures 5 and 6 for all problems. Note that in the free cylinder $\sigma_r = \sigma_\vartheta = p$ as anticipated from theory. Thus for problem 1 the three main normal tensions are compressive tensions and are equal to p. By distinction, in both the constrained cylinder and the reservoir σ_r and σ_ϑ exhibit a similar behaviour and their value amounts to 0·33p. Again a small region around the reservoir boundary has to be excluded as there σ_r achieves a value in excess of 0·33p (Figure 5). Figures 7–9 indicate the substantial uniformity of σ_r and σ_ϑ with z and, similarly to σ_z, their vanishing outside the reservoir (Figure 9). It is worth noting the similarity of σ_r and σ_ϑ in the reservoir and the constrained cylinder. In both problems the confinement factor $k = \sigma_r/\sigma_z$ turns out to be $k = \nu/(1 - \nu) = 0{\cdot}33$, i.e. the theoretical value experienced at the much smaller scale of an oedometer cell.

3.3. *Shear stress* τ_{rz}

The behaviour of shear stress τ_{rz} in problems 1 and 2 is different from that of problem 3 and the analogy found for the normal stresses does no more hold for the shear stress. Figure 10 shows that in both the free and the constrained cylinder a uniform pore pressure decline does not induce the development of shear stress. By contrast, Figure 11 reveals that shear stresses generate close to the reservoir boundary both inside and outside the field with a peak τ_{rz} value of the same order

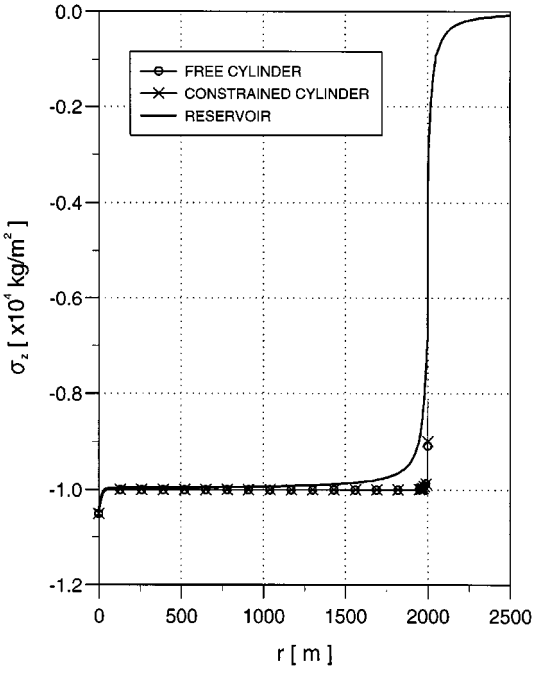

Figure 2. Vertical stress σ_z vs. r on the median plane of reservoir and equivalent porous cylinders

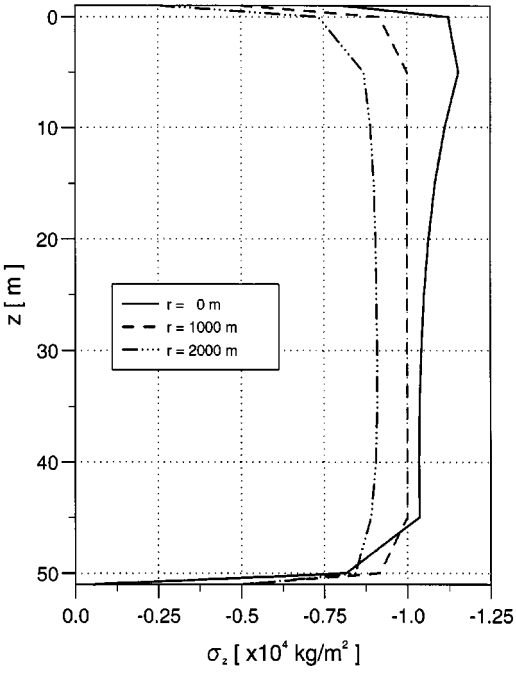

Figure 3. Vertical stress σ_z vs. z at various distances r from the symmetry axis (problems 1 and 2)

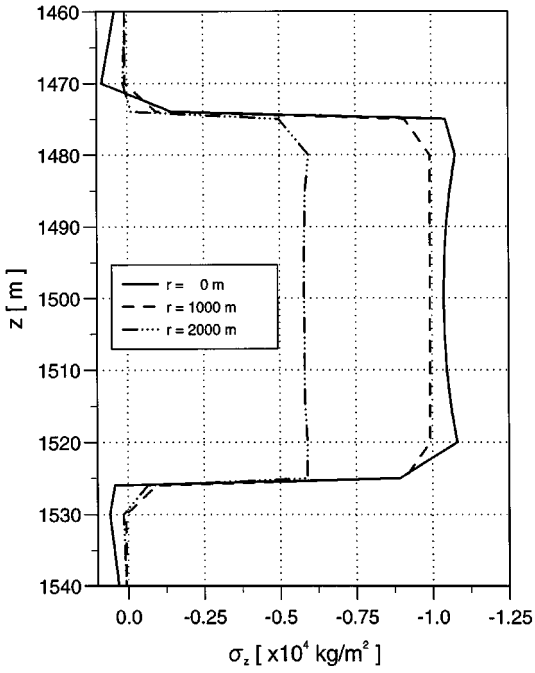

Figure 4. The same as in Figure 3 for problem 3

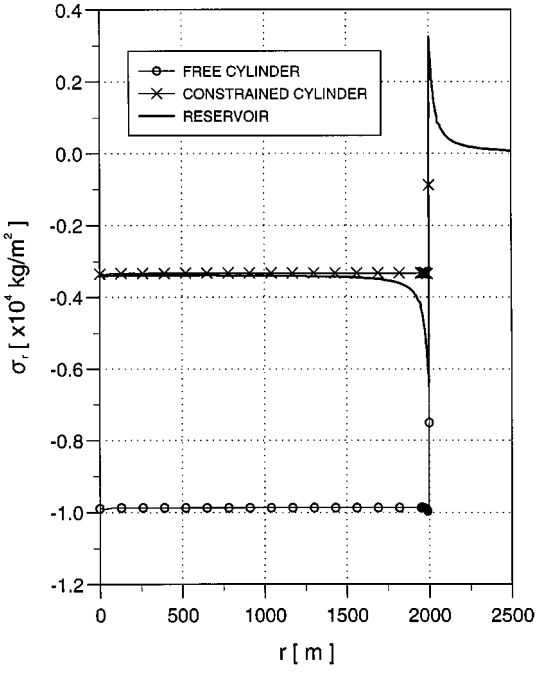

Figure 5. Radial stress σ_r vs. radial distance r on the median plane of reservoir and equivalent porous cylinders

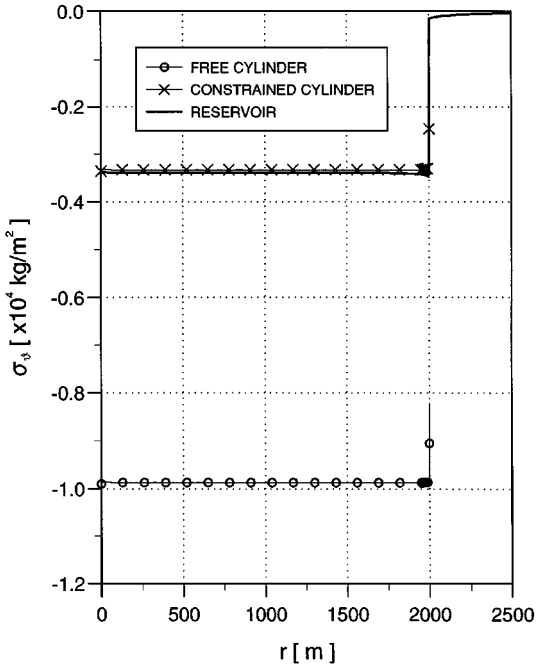

Figure 6. The same as Figure 5 for tangential stress σ_ϑ

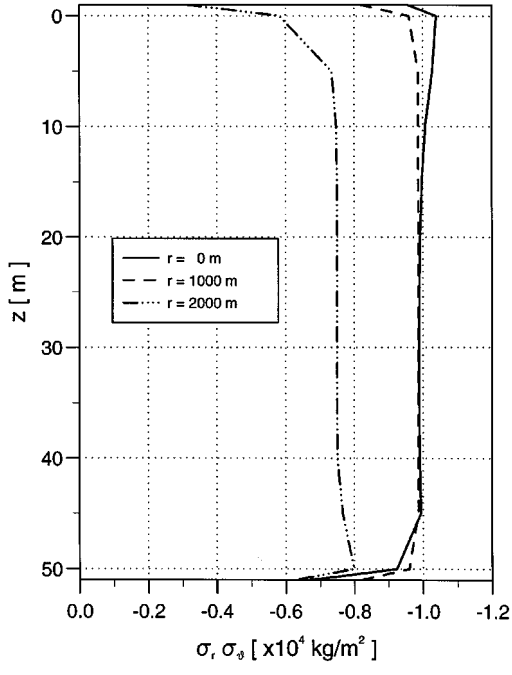

Figure 7. Radial stress σ_r and tangential stress σ_ϑ vs. z at various distances r from the symmetry axis (problem 1)

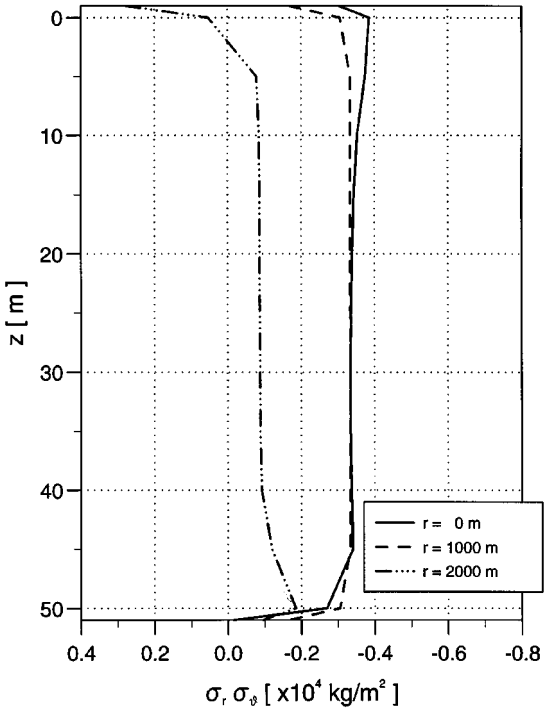

Figure 8. The same as in Figure 7 for problem 2

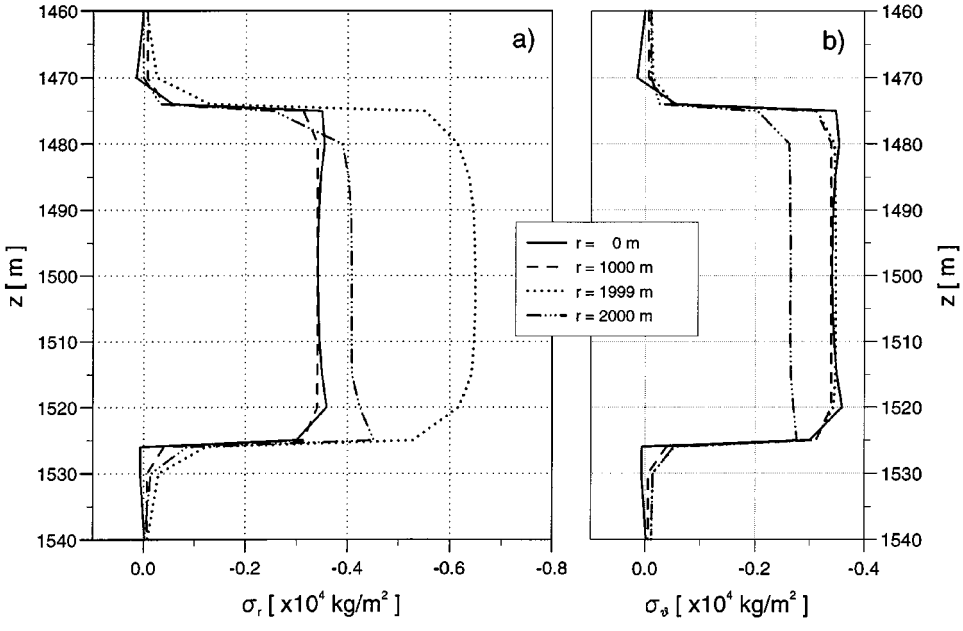

Figure 9. Radial stress σ_r (a) and tangential stress σ_ϑ (b) vs. z at various distances r from the symmetry axis (problem 3)

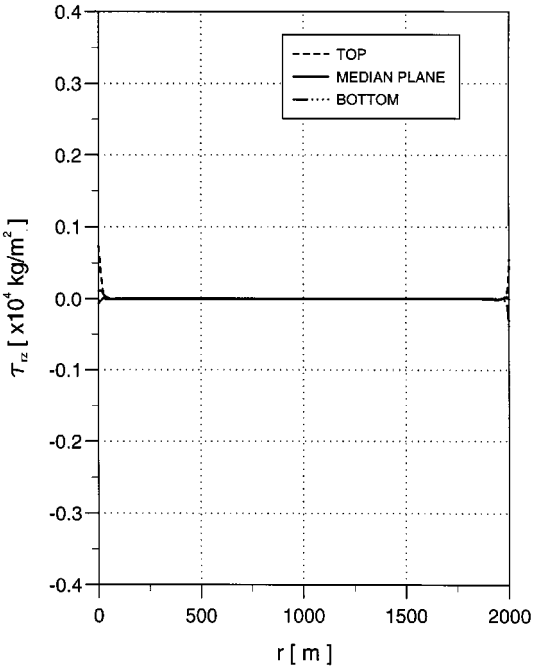

Figure 10. Shear stress τ_{rz} vs. radial distance r (problems 1 and 2)

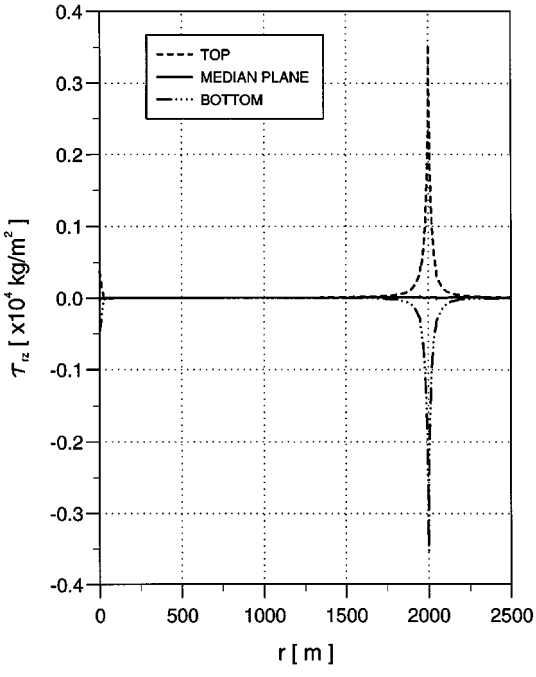

Figure 11. The same as in Figure 10 for problem 3

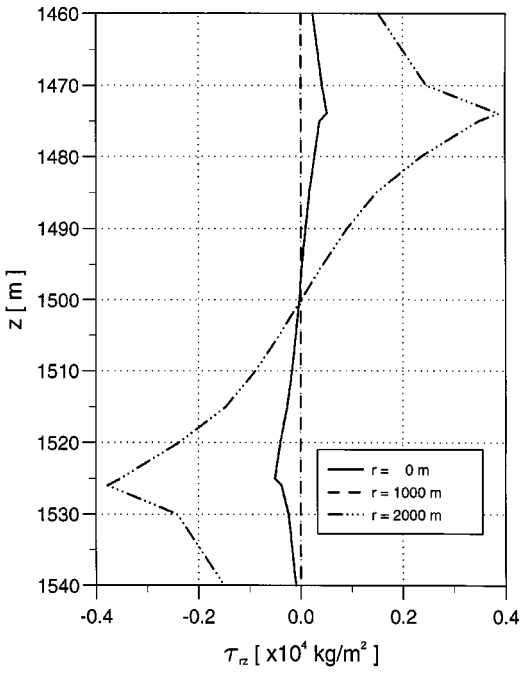

Figure 12. Shear stress τ_{rz} vs. z at various distances r from the symmetry axis (problem 3)

of magnitude as σ_r and σ_ϑ. Note in Figure 12 that τ_{rz} is not uniform with z and its sign changes on the median reservoir plane.

3.4. *Discussion on stress state*

We can summarize the state of stress generated by a pressure decline $p = -10^4$ kg/m^2 by recalling that in a free cylinder (problem 1) the stress distribution is isotropic with $\sigma_z = \sigma_r = \sigma_\vartheta = p$ and $\tau_{rz} = 0$. The laterally constrained cylinder and the reservoir embedded in a half-space are quite similar as far as the normal stresses are concerned: $\sigma_z = p$, $\sigma_r = \sigma_\vartheta = 0{\cdot}33p$, $k = \nu/(1-\nu)$ throughout the reservoir except in a small region with $r \sim R_e$ where k exceeds the theoretical value (Figure 13). As regards to τ_{rz}, in the inner part of the reservoir we have $\tau_{rz} = 0$ as in an oedometer cell. Close to the field edge, however, large shear stresses develop which are comparable to the normal horizontal stresses.

3.5. *Vertical displacement u_z and compaction δ*

The vertical reservoir compaction is defined as

$$\delta = u_{z,\mathrm{TOP}} - u_{z,\mathrm{BOTTOM}}$$

i.e. equal to the difference between the vertical top and bottom displacements. The analysis shows that δ is equal to the compaction of the equivalent constrained cylinder (for which $\delta = u_{z,\mathrm{TOP}}$).

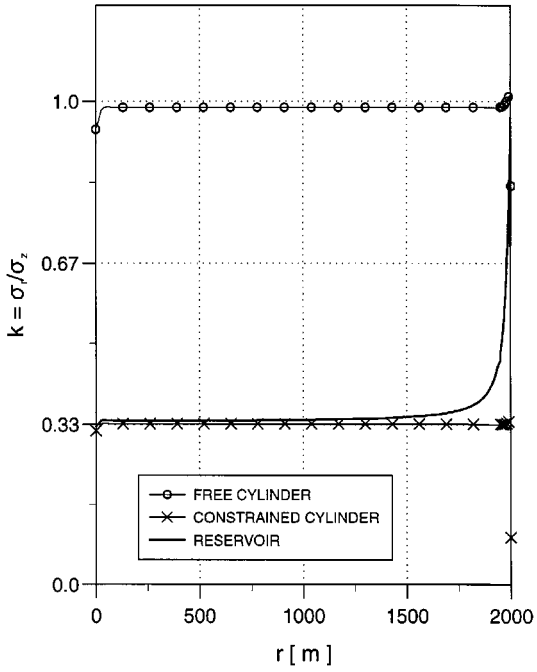

Figure 13. Confinement factor $k = \sigma_r/\sigma_z$ vs. radial distance r

This is evidenced in Figure 14 yielding δ and $u_{z,\mathrm{TOP}}$ for problems 1 and 2. Note that for the free cylinder $u_{z,\mathrm{TOP}} \sim 0{\cdot}3$ m, i.e. equal to the theoretical value

$$u_{z,\mathrm{TOP}} = \frac{1}{E}\left[\sigma_z - \nu(\sigma_r + \sigma_\vartheta)\right] l = 0{\cdot}306 \text{ m}$$

which is obtained using a sample length $l = h + \frac{1}{2}(2s_{\mathrm{V}}) = 51$ m and a Young modulus $E = (1 + \nu)(1 - 2\nu)/\alpha(1 - \nu) = 0{\cdot}8\overline{3} \times 10^6$ kg/m^2. By distinction, for problems 2 and 3 the compaction is different from that of the unconstrained cylinder. For these we have (Figure 14):

$$\delta = \alpha\sigma_z l = \alpha p l = 0{\cdot}51 \text{ m}$$

Toward the outer reservoir boundary δ decreases, it becomes half the above value at $r = R_e$ and quickly vanishes for $r > R_e$.

Thus, the assumption that the reservoir compacts similarly to an oedometer sample is correct for most of its horizontal extent. Compaction becomes smaller only in a limited region close to the field boundary.

3.6. Horizontal displacement u_r

In a free cylinder u_r grows linearly with r (Figure 15(a)) with its maximum value achieved at $r = R_e$. The outcome of Figure 15(a) is consistent with theory which for a thin disc-shaped body

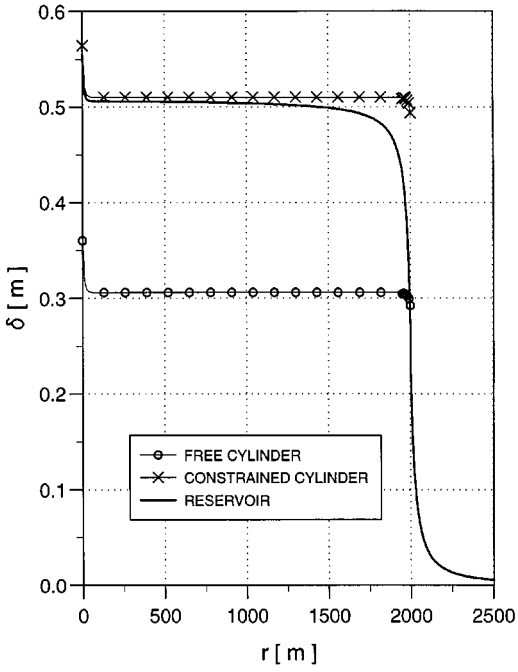

Figure 14. Vertical compaction δ of the reservoir and the equivalent porous cylinder vs. radial distance r

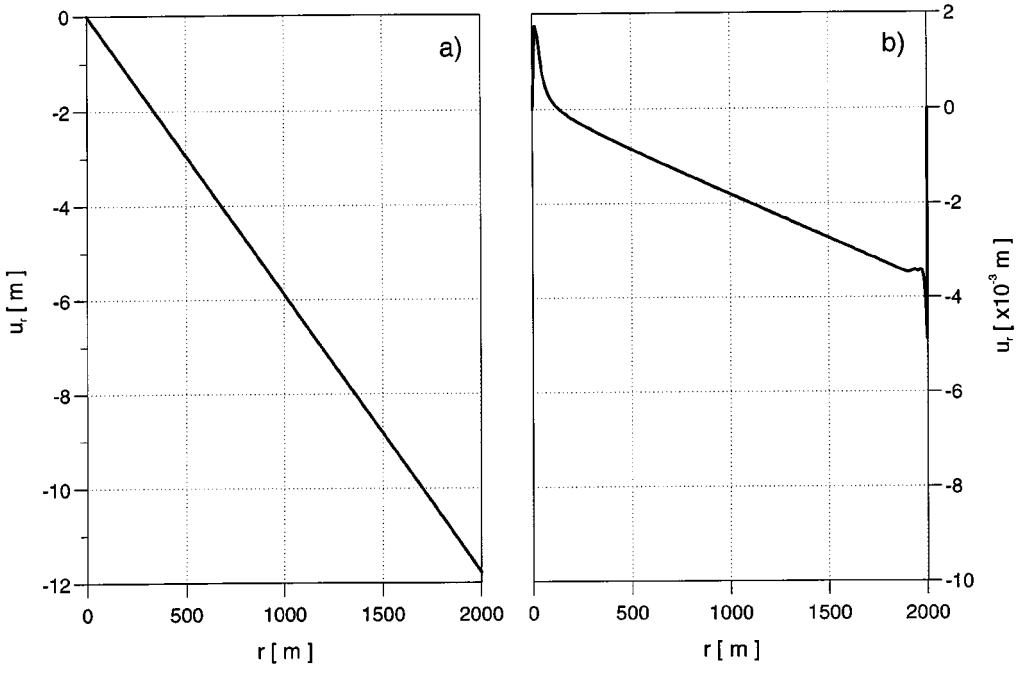

Figure 15. Horizontal displacement u_r vs. r on the median plane of the free (a) and constrained (b) equivalent porous cylinders (problems 1 and 2)

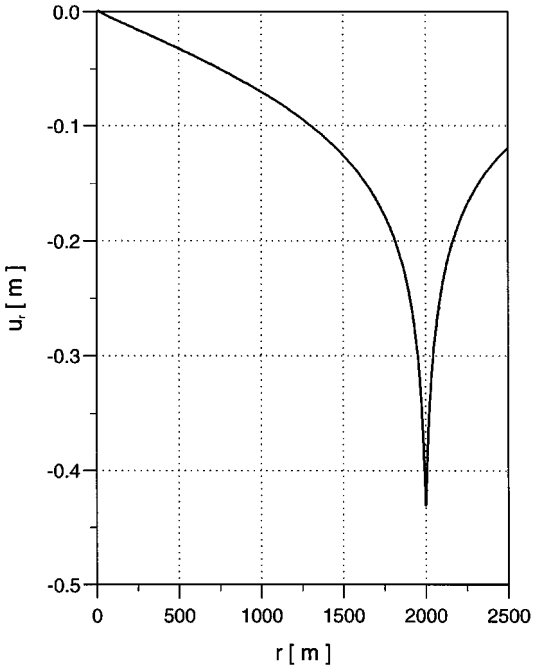

Figure 16. Horizontal displacement u_r vs. r on the median plane of the reservoir (problem 3)

subject to an isotropic state of stress predicts the radial displacement as

$$u_r = \frac{1-2v}{E}\, pr = \frac{1-v}{1+v}\, \alpha pr = -0{\cdot}6 \times 10^{-2} r$$

In a constrained cylinder (problem 2) u_r is negligible for any r (Figure 15(b)) and becomes zero at $r = 0$ and $r = R_e$. Inside the cylinder u_r increases linearly with r and achieves its largest value of few millimeters close to $r = R_e$.

The behaviour of u_r within a reservoir is quite different from that of the equivalent oedometer experiment, as may be seen in Figure 16 showing that u_r does not vary linearly with r and attains its maximum value at $r = R_e$. This value is small compared to the corresponding displacement of the free cylinder (Figure 15(a)). However, it turns out to be of the same order of magnitude as δ. Note in Figure 16 that u_r becomes significant close to the reservoir boundary where the state of stress mostly deviates from that of the confined cylinder, with the confinement factor k getting larger than the oedometer value 0·33, and the generation of important shear stresses. Actually, these stresses contribute to the development of appreciable horizontal displacements in productive reservoirs.

3.7. Strain components

We analyse the behaviour of the strain components $\varepsilon_z = \partial u_z/\partial z$ and $\varepsilon_r = \partial u_r/\partial r$ for the three sample problems. As the normal stresses are uniform with z we restrict our study to the results on

Table I. Strain components ε_z and ε_r (problems 1 and 2)

Problem	ε_z	ε_r
1	6×10^{-3}	6×10^{-3}
2	10^{-2}	2×10^{-6}

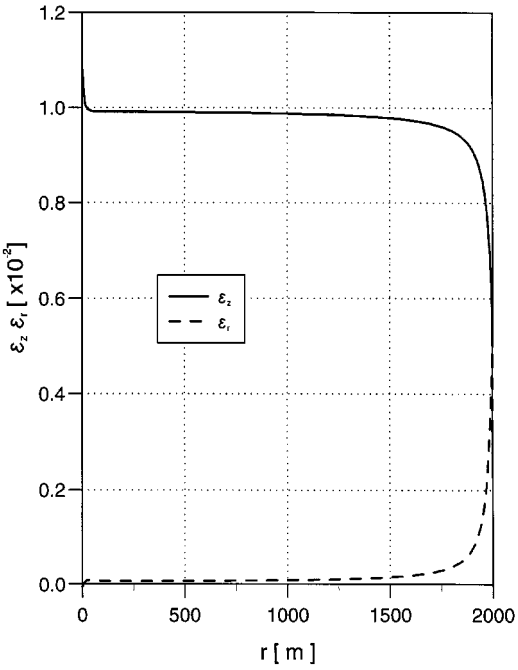

Figure 17. Absolute value of vertical and radial components ε_z and ε_r of volume strain vs. radial distance r (problem 3)

the median plane of the reservoir and the equivalent cylinders. The components ε_z is evaluated as the ratio between δ and $l = h + s_V$. In problem 2, ε_r is computed using u_r where u_r exhibits a linear behaviour. The outcome of problems 1 and 2 are independent of r and are summarized in Table I. The results of problem 3 are a function of r and are given in Figure 17. Note that ε_z varies from the largest value of 10^{-2}, which is practically constant for $r \leqslant 1500$ m, to the minimum value half-time as much, while ε_r is approximately equal to 10^{-4}, except for the boundary region where it grows up to $0{\cdot}5 \times 10^{-2}$.

Careful consideration of the previous results shows that, as far as the deformation is concerned, a reservoir during its production life can be divided into two regions characterized by a different behaviour:

(1) the inner region, which extends to a distance from the boundary equal to a few times the thickness h, where ε_z is the same as that of the equivalent confined cylinder, while ε_r is orders

of magnitude smaller than ε_z and takes on an intermediate value between the radial strains of the free and the constrained cylinders;

(2) the region near the boundary, whose horizontal size is few times h, where $\varepsilon_r/\varepsilon_z$ progressively increases with r and achieves unity at $r = R_e$.

3.8. Influence of the reservoir depth of burial

The previous discussion shows that a thin reservoir from a mechanical viewpoint basically behaves like a constrained cylindrical porous medium except for a limited region in the vicinity of the boundary. We wish now to explore the influence of burial depth c on the results by setting $c = 26$ m (surface reservoir), $c = 100$ m (shallow reservoir), and $c = 3000$ m (deep reservoir).

Figures 18–20 provide evidence that σ_z, σ_r and σ_ϑ are independent of c. A less than 10% difference may be observed close to the field boundary. This remark holds true for the shear stress τ_{rz} as well (Figure 21). However, for the surface reservoir (whose top is located 1 m below the land surface) τ_{rz} appears to be negligibly small on the reservoir top (Figure 21).

By distinction, the deformation is more sensitive to c. This is so because the shape and volume of the neighbouring medium which opposes the reservoir contraction changes with c. The most interesting results are reported in Figures 22–24. Observe in Figures 22 and 23 that $u_{z,\mathrm{TOP}}$, $u_{z,\mathrm{BOTTOM}}$ and u_r are much influenced by c and in Figure 24 that u_r in surface and shallow formations is not uniform with z at $r = R_e$ (for the ease of interpretation the u_r profiles are provided against $z' = c - z$). The displacement u_r here is not symmetric with respect to the

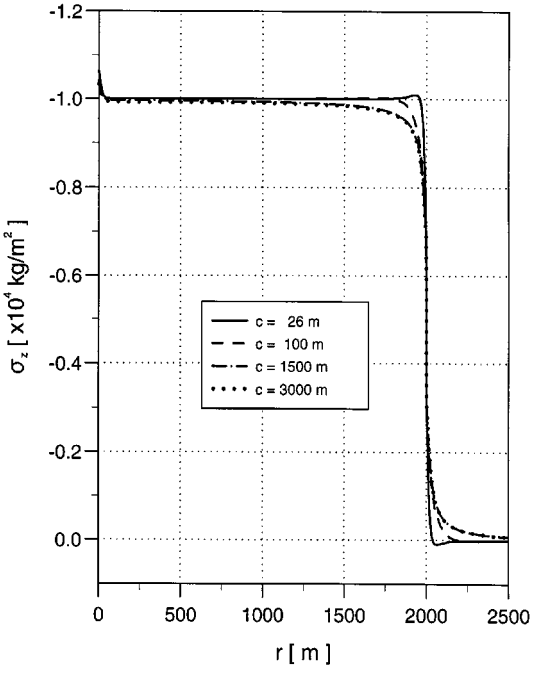

Figure 18. Vertical stress σ_z vs. radial distance r on the median reservoir plane for various burial depths c

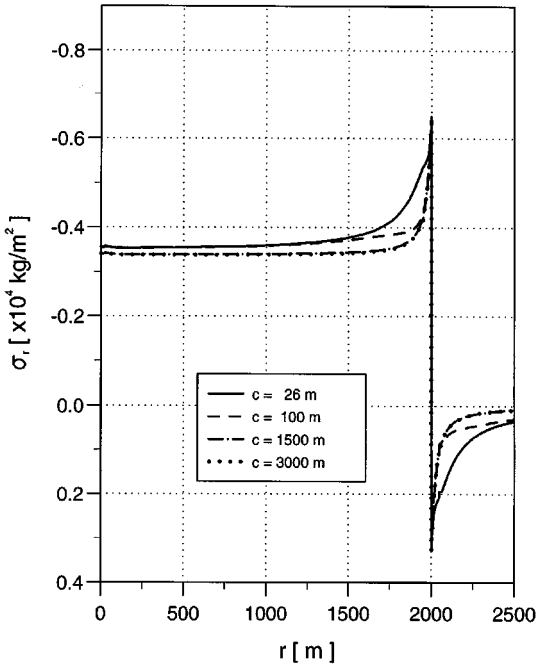

Figure 19. The same as in Figure 18 for the radial stress σ_r

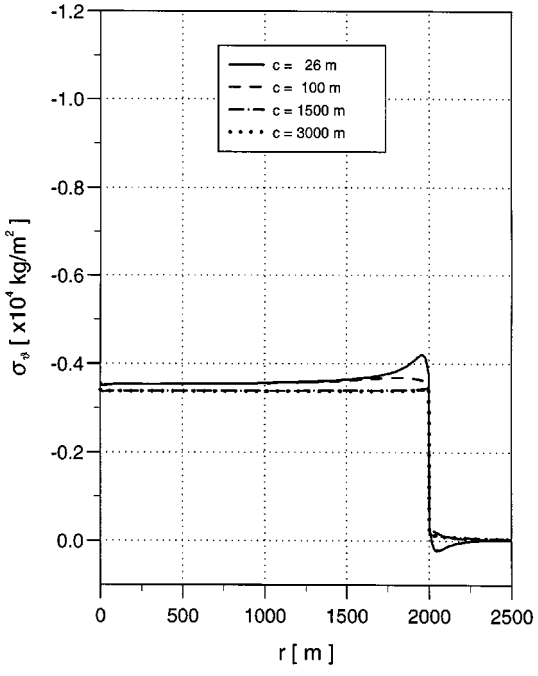

Figure 20. The same as in Figure 18 for the tangential stress σ_ϑ

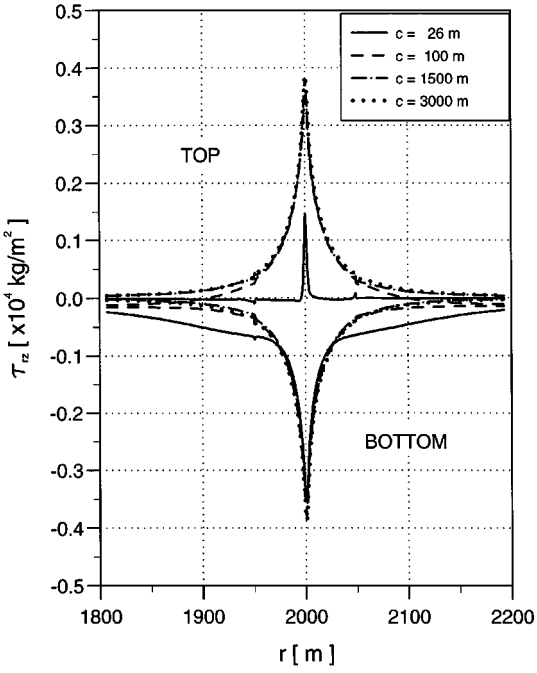

Figure 21. Shear stress τ_{rz} on the reservoir top and bottom vs. radial distance r for various burial depths c

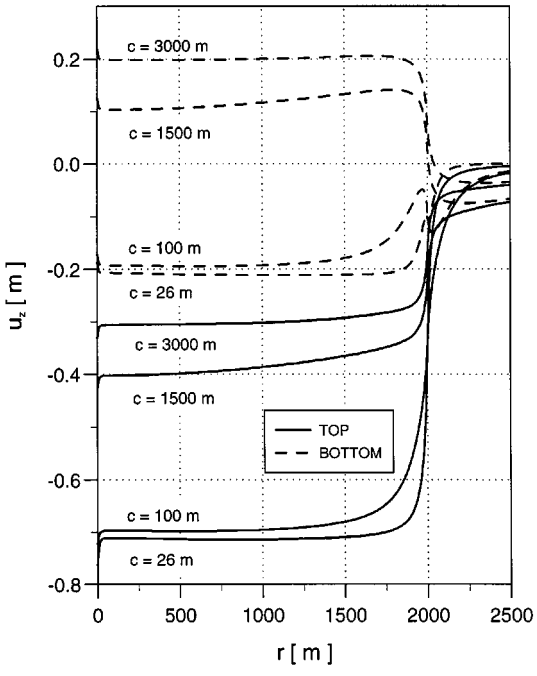

Figure 22. Vertical displacement u_z of the reservoir top and bottom vs. radial distance r for various burial depths c

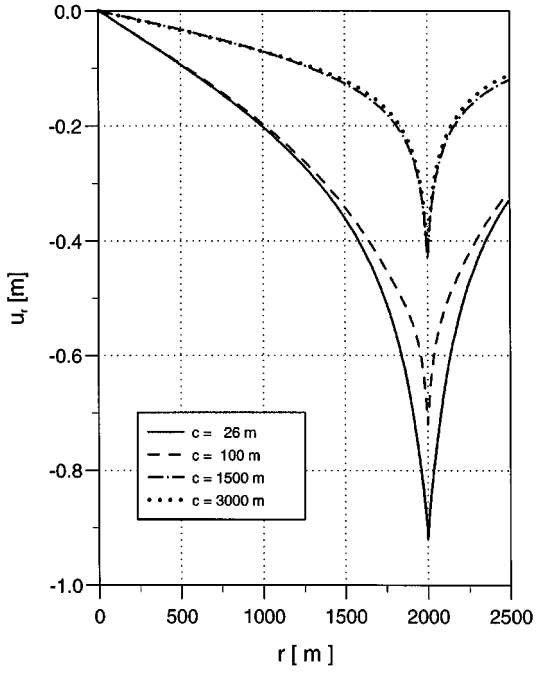

Figure 23. Horizontal displacement u_r on the median reservoir plane vs. radial distance r for various burial depths c

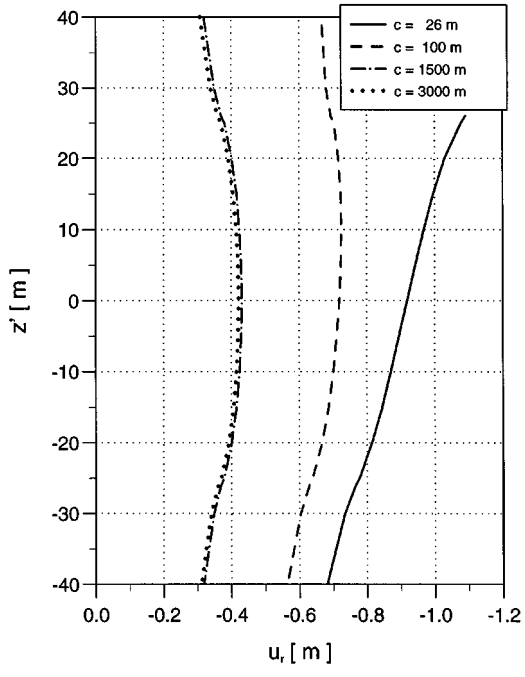

Figure 24. Horizontal displacement u_r vs. $z' = c - z$ at the reservoir boundary ($r = R_e$) for various burial depths c

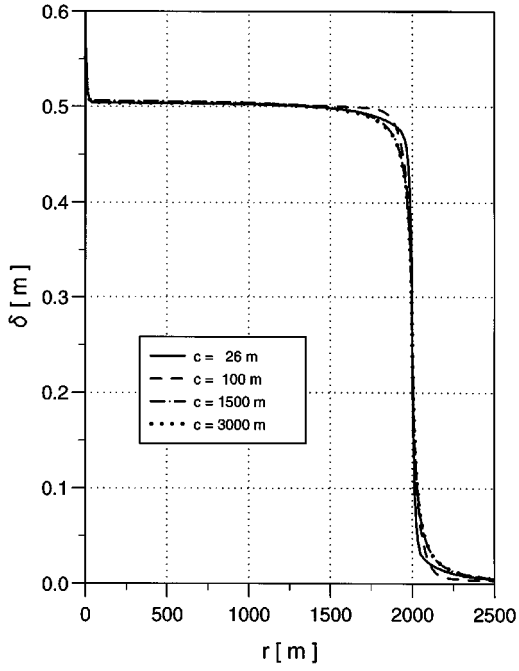

Figure 25. Reservoir vertical compaction δ vs. radial distance r for various burial depths c

median reservoir plane. Symmetry is recovered in deeper fields (Figure 24). Also note that for $c = 1500$ m the behaviour of u_r (Figures 23 and 24) is pretty much the same as that obtained for $c = 3000$ m which in turn approaches the behaviour of a reservoir embedded in an infinite medium. The asymptotic behaviour holds for u_z as well (Figure 22) but convergence to the $c = \infty$ solution is slower.

Although the vertical displacements are related to c (Figure 22), nevertheless compaction δ does not depend on c (Figure 25). This result is very important as it indicates that the reservoir compaction is not influenced by the depth of burial, i.e. that the oedometer analogy holds irrespective of burial depth. As regards to ε_r, Figure 23 shows that, although variable with r, ε_r takes on values which are of the same order of magnitude for different c. Therefore $\varepsilon_z \gg \varepsilon_r$ in general except for the reservoir boundary region.

3.9. Influence of pore pressure gradient

We again assume $c = 1500$ m and analyse the stress state for different s_L values ($s_L = 1$, 10 and 50 m). Increasing s_L implies a less steep pressure gradient outside the reservoir, i.e. a smaller body force per unit volume generated by pressure dissipation. The sensitivity of stresses to s_L is shown in Figures 26–29. Note in Figures 26 and 28 that σ_z and σ_ϑ do not vary with s_L. The radial stress σ_r is also independent of s_L except for the peak value at $r = R_e$ which is less pronounced for the largest s_L value (Figure 27). By distinction, τ_{rz} is markedly influenced by s_L (Figure 29). A larger s_L, that is a smaller gradient, produces a flattening of the shear stress profile, hence a smaller

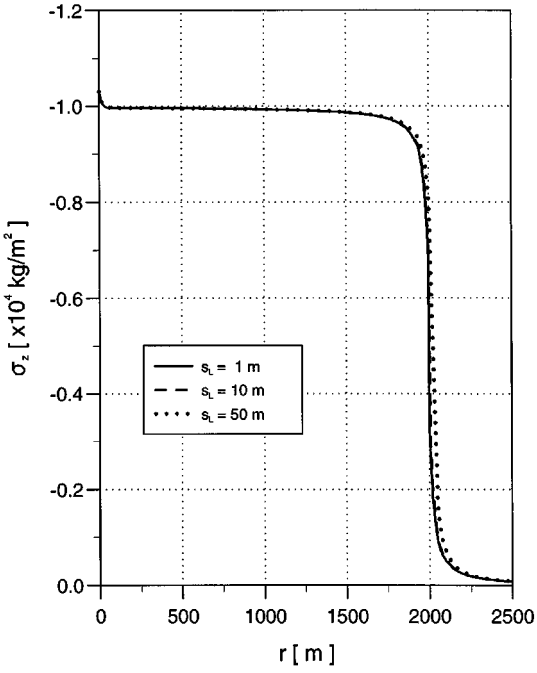

Figure 26. Vertical stress σ_z vs. radial distance r on the median reservoir plane for various s_L values

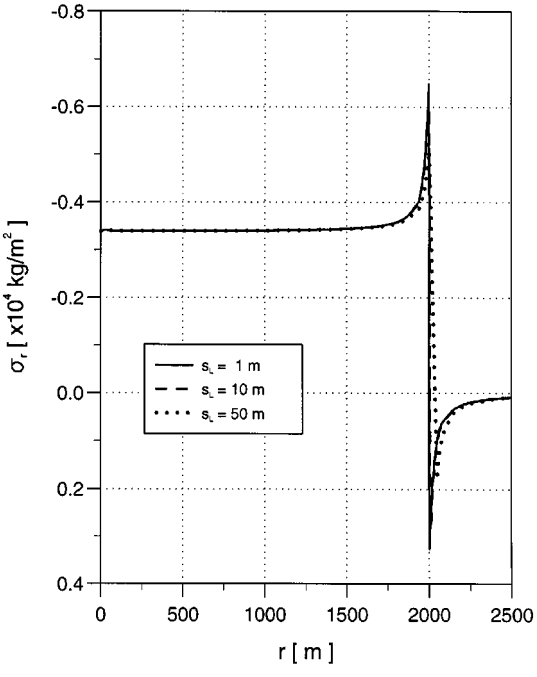

Figure 27. The same as Figure 26 for the radial stress σ_r

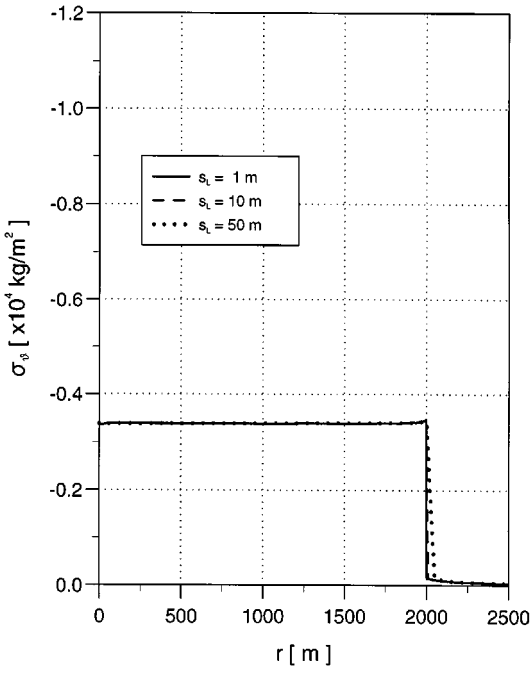

Figure 28. The same as Figure 26 for the tangential stress σ_ϑ

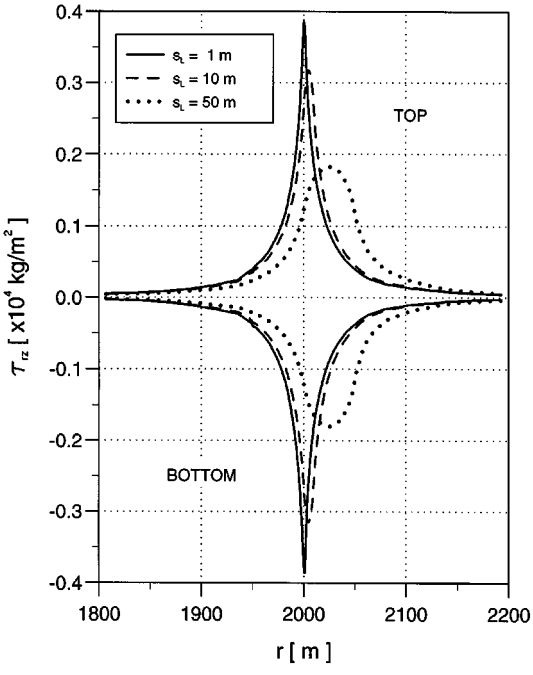

Figure 29. Shear stress τ_{rz} on the reservoir top and bottom vs. radial distance r for various s_L values

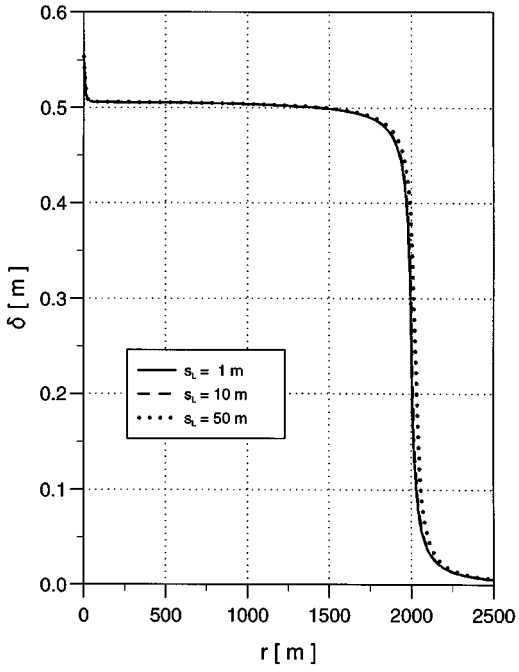

Figure 30. Reservoir vertical compaction δ vs. radial distance r for various s_L values

probability of rock failure, fault reactivation and ground cracks that may be generated at the field margin (these cracks were first noticed over the Goose Creek oil field in Texas, see Reference 20). For the influence of shear stress on triggering earthquakes, see Reference 21.

Finally Figures 30 and 31 provide δ and u_r vs. r for the three selected s_L values. The differences in these profiles are really small and we may conclude that both reservoir vertical compaction and horizontal displacement are not affected by s_L, i.e. the volume over which the pore pressure decline dissipates.

4. CONCLUSIONS

A stress–strain analysis in a thin disc-shaped reservoir embedded in a semi-infinite medium has been performed using a finite element model. The study has been extended to the neighbouring rocks as well and a comparison has been made with the geometrically equivalent poro-elastic cylinder which is either free to or prevented from expanding laterally (oedometer analogy) and experiences the same pore pressure decline as the reservoir. The influence of burial depth and pressure gradient has also been investigated.

As anticipated, the results show a few basic similarities between the reservoir mechanical behaviour and the behaviour of the confined cylinder which hold throughout the gas/oil field except in a limited region close the reservoir edge. These similarities concern the normal stresses and the compaction, i.e.:

(1) In both the reservoir and the confined cylinder the normal stresses σ_z, σ_r and σ_ϑ are pretty much the same along with the confinement factor $k = \sigma_n/\sigma_z = \nu/(1 - \nu)$;

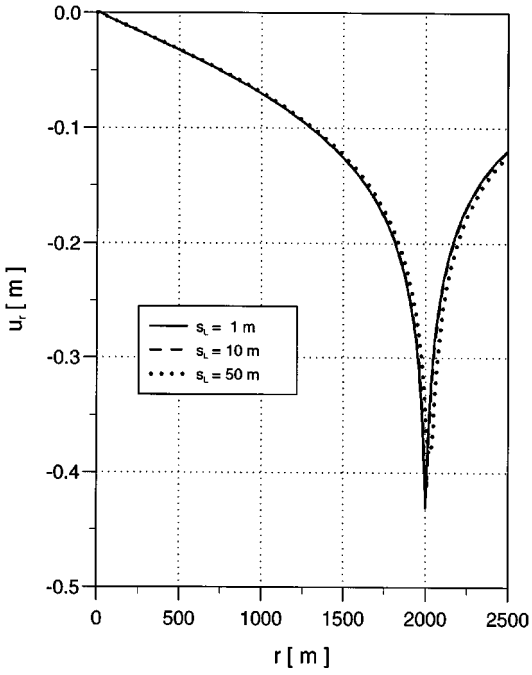

Figure 31. The same as Figure 30 for the horizontal displacement u_r

(2) the vertical compaction δ of the depressurized rocks in the same in both problems and is equal to αhp.

Hence it is confirmed that oedometer tests are the most appropriate tests for the assessment of the vertical gas/oil field compressibility α since the stress path experienced by the reservoir sediments is well reproduced in an oedometer cell.

The study has also focused on the deviations from the oedometer experiment:

(1) the generation of shear stresses close to the reservoir boundary with a peak value at $r = R_e$ of the same order of magnitude as the normal horizontal stresses;
(2) the development of a non-negligible displacement u_r caused by both the shear stress and a reduced radial tensile stress right beyond the field edge. Displacement u_r gives rise to a strain ε_r much smaller than ε_z but much larger than the radial strain of the confined cylinder.

Further investigation has pointed out that:

(1) both stresses and reservoir compaction are insensitive to burial depth c while the vertical and the horizontal displacements in the reservoir are much dependent on c, especially in shallow gas/oil bearing formations. As c increases, u_r and u_z approach the asymptotic value which characterizes a reservoir embedded in an infinite medium (almost achieved for $c = 3000$ m in the example dealt with in the present study);

(2) as s_L increases, i.e. as the pore pressure gradient reduces, the maximum τ_{rz} and σ_r at the field edge become smaller and spread over a larger volume, while σ_z, σ_ϑ, δ and the medium deformation remain unchanged.

ACKNOWLEDGEMENTS

This research was supported by the EC Environment Research Programme (contract: EV5V-CT94-0498, Climatology and Natural Hazards).

REFERENCES

1. J. P. Johnson, D. W. Rhett and W. T. Slemers, 'Rock mechanics of the Ekofisk reservoir in the evaluation of subsidence', *JPT*, **41**(7), 717–722 (1989).
2. I. Ruddy, M. A. Andersen, P. D. Pattillo, M. Bislawi and N. Foged, 'Rock compressibility, compaction, and subsidence in a highly-porosity chalk reservoir: A case study of Valhall field, *JPT*, **41**(7), 741–746 (1989).
3. J. Geertsma, 'Problems of rock mechanics in petroleum production engineering', *Proc. 1st Cong. Int. Soc. Rock Mechan.,* Lisbon, 1966, pp. 585–594.
4. J. Geertsma, 'Land subsidence above compacting oil and gas reservoir, *JPT*, **25,** 734–744, 1973a.
5. G. Gambolati, 'A three-dimensional model to compute land subsidence', *IAHS Bull*., **17**(2), 219–226 (1972).
6. O. C. Zinkiewicz, *The Finite Element Method*, 3rd edn, McGraw-Hill, New York, 1977.
7. G. Gambolati, G. Gatto and G. Ricceri, 'Land subsidence due to gas–oil removal in layered anisotropic soils by a finite element model', *Proc. 3rd Int. Symp. Land Subsidence*, IAHS Publ. No. 151, Wallingford, UK, 1984, pp. 29–41.
8. G. Gambolati, G. Ricceri, W. Bertoni, G. Brighenti and E. Vuillermin, 'Mathematical simulation of the subsidence of Ravenna', *Water Resour. Res*., **27**(11), 2899–2918 (1991).
9. G. Gambolati, P. Teatini and W. Bertoni, 'Numerical prediction of land subsidence over Dosso degli Angeli gas field, Ravenna, Italy', in J. Borchers (ed.), Land Subsidence—Current Research and Case Studies, *Proc. of the J. F. Poland Symp. Land Subsidence*, 229–238. Star Publ. Co., Belmonton (CA) 1998.
10. J. Geertsma, 'A basic theory of subsidence due to reservoir compaction: The homogeneous case', in *The Analysis of Surface Subsidence Resulting from Gas Production in the Groningen Area, the Netherlands*, Nederlandse Aardolie Maatschappij, 1973b, pp. 43–62.
11. J. Geertsma and G. van Opstal, 'A numerical technique for predicting subsidence above compacting reservoirs based on the nucleus of strain concepts', in: *The Analysis of Surface Subsidence Resulting from Gas Production in the Groningen Area, the Netherlands*, Nederlandse Aardolie Maatschappij 1973, pp. 63–78.
12. D. Kosloff, R. F. Scott and J. Scranton, Finite element simulation of Wilmington oil field subsidence: 1. Linear modelling', *Tectonophysics*, **65,** 339–368 (1980).
13. J. C. Martin and S. Serdengecti, 'Subsidence over oil and gas fields', in *Man-Induced Land Subsidence*, *Rev. Eng. Geol*., Vol. VI, Boulder (CO), Geol. Soc. of America, 1984, pp. 23–34.
14. F. B. J. Barends, F. J. J. Brouwer and F. M. Schröder (eds), Land Subsidence, *Proc. V Int. Symp. Land Subsidence*, *The Hague*, *October 95*, IAHS Publ. No. 234, Wallingford, 1995, 492 pp.
15. E. C. Donaldson, G. V. Chilingarian and H. H. Rieke, 'Stresses in sediments', in G. V. Chilingarian et al. (ed.), *Subsidence due to fluid withdrawal*, Developments in Petroleum Science, Vol. 41, Elsevier, Amsterdam, 1995, pp. 165–192.
16. NAM, 'Subsidence caused by natural gas production', *Report 27600*, *Nederlandse Aardolie Maatschappij*, *Assen*, The Netherlands, 1995, 26 pp.
17. A. Verruijt, 'Elastic storage of aquifers', in R. De Wiest (ed.), *Flow Through Porous Media*, Academic, New York, 1969, pp. 331–376.
18. G. Gambolati, 'Second-order theory of flow in three-dimensional deforming media', *Water Resour. Res*., **10**(6), 1217–1228 (1974).
19. E. Detournay and A. H.-D. Cheng, 'Fundamentals of poro-elasticity', in C Fairhurst (ed.), *Comprehensive Rock Engineering: Principles, Practice & Projects, Vol. II, Analysis and Design Method*, Pergamon Press, 1993, pp. 113–171.
20. W. E. Pratt and D. W. Johnson, 'Local subsidence of the Goose Creek oil field', *J. Geology*, **XXXIV**(7) (Part 1), 577–590 (1926).
21. F. B. J. Barends, J. T. van der Poel and J. A. M. Teunissen, 'Geomechanical simulation of static and dynamic subsidence by reservoir compaction', in F. B. J. Barends et al. (ed.), *Land Subsidence*, *Proc. V Int. Symp. Land Subsidence*, *The Hague*, *October 95*, 237–245, A. A. Balkema Publ., Rotterdam, 1995.

